Resonant dielectric multilayer with controlled absorption for enhanced total internal reflection fluorescence microscopy

A Mouttou, F Lemarchand, C Koc, A Moreau, J Lumeau, C Favard, Aude L. L. Lereu

Research Article | Vol. 30, No. 9 / 25 Apr 2022 / Optics Express 15365
Optics EXPRESS

Resonant dielectric multilayer with controlled absorption for enhanced total internal reflection fluorescence microscopy

A. Mouttou,[1,2] F. Lemarchand,[2] C. Koc,[2] A. Moreau,[2] J. Lumeau,[2] C. Favard,[1,3] and A. L. Lereu[2,4]

[1]Institut de Recherche en Infectiologie de Montpellier, CNRS, Univ of Montpellier, Montpellier, France
[2]Aix Marseille Univ, CNRS, Centrale Marseille, Institut Fresnel, Marseille, France
[3]cyril.favard@irim.cnrs.fr
[4]aude.lereu@fresnel.fr

Abstract: Total internal reflection fluorescence microscopy (TIRF-M) is widely used in biological imaging. Evanescent waves, generated at the glass-sample interface, theoretically strongly improve the axial resolution down to a hundred of nanometers. However, objective based TIRF-M suffers from different limitations such as interference fringes and uneven illumination, mixing both propagating and evanescent waves, which degrade the image quality. In principle, uneven illumination could be avoided by increasing the excitation angle, but this results in a drastic loss of excitation power. We designed dedicated 1D photonic crystals in order to circumvent this power loss by directly acting on the intensity of the evanescent field at controlled incident angles. In this framework, we used dedicated resonant multi-dielectric stacks, supporting Bloch surface waves and resulting in large field enhancement when illuminated under the conditions of total internal reflection. Here, we present a numerical optimization of such resonant stacks by adapting the resulting resonance to the angular illumination conditions in TIRF-M and to the fluorescence collection constraints. We thus propose a dedicated resonant structure with a control of the absorption during thin film deposition. A first experimental demonstration illustrates the concept with a 3-fold fluorescence enhancement in agreement with the numerical predictions.

1. Introduction

Total Internal Reflection Fluorescence Microscopy (TIRF-M) is a widely used, commercially available, imaging technique in biology labs. TIRF-M is based on the generation of evanescent waves allowing the improvement of the microscope axial resolution down to hundreds of nanometers at the sample/coverslip interface [1]. Recent coupling of TIRF-M to single molecule techniques such as PALM (PhotoActivation Localization Microscopy) [2] and STORM (STochastic Optical Reconstruction Microscopy) [3] has lead to its resurgence of cellular biology and recently virology [4–8]. It has also recently been coupled to super-critical angle fluorescence detection, allowing unprecedentedly achieved axial resolution and localisation precision [9]. All of the commercially available TIRF microscopes nowadays use high numerical aperture ($NA \geq 1.45$) objectives to reach the necessary angle for total internal reflection of the excitation beam at the glass coverslip-biological interface (with n_{Bio}=1.35, $\theta \geq \theta_c = 62.8°$), these are so-called "objective based TIRF-microscopes". Different sources of noise can affect the optical contrast of these objective based TIRF-microscopes. For example, as the evanescent field intensity maximum occurs at the critical angle $\theta_c = 62.8°$, due to the intrinsic large beam divergence (classically above 0.5°), excitation at this angle will let far-field excitation to penetrate the sample, drastically deteriorating the contrast and axial resolution [10,11]. A simple way to circumvent this problem is to increase the incident angle of the excitation beam, which unfortunately results in a rapid decrease of the evanescent field intensity, leading again to a poor contrast.

#457353 https://doi.org/10.1364/OE.457353
Journal © 2022 Received 3 Mar 2022; accepted 4 Apr 2022; published 20 Apr 2022

Optics EXPRESS

However, evanescent intensity can be enhanced using extreme or ultimate confinements of electromagnetic fields at the interface. More precisely, thin film-based nanophotonic is one of the most well-established field where the evanescent waves (EW) are mainly investigated and controlled for EW-sensing [12] and references therein or EW-imaging [11] and references therein. For the sake of improving EW microscopy efficiency, Lakowicz et al introduced, in 2004, the Surface Plasmon-Coupled Emission (SPCE) using metallic thin films supporting surface plasmon (SPs) resonances and evidencing a large improvement over the collected fluorescence signal [13,14]. The SPCE was then observed by leakage radiation microscopy evidencing the coupling between the SPs and the fluorescence molecules [15]. In the same time, SP mediated fluorescence microscopy (SPMFM) for cells imaging [16], based on a prismless total internal reflection fluorescence microscopy (TIRFM), reported a fluorescence enhancement of 3 together with an increase of the signal-to-noise ratio by a factor of 1.5 [17]. However, these techniques suffer from illumination conditions limitations linked to the metal intrinsic properties, from quenching effects of the fluorophores in the vicinity of metals and are not highly biocompatible.

To overcome these issues, Bloch surface waves-coupled emission (BSWCE) using planar resonant dielectric multilayer (DM) was introduced in [18–25]. Since then, numerous works have established comparisons between SPs and BSWs evidencing the advantages and drawbacks for both mechanisms [26–29]. More precisely, in the framework of fluorescence imaging, early works [25,30] evidence above 5-fold increase in fluorescence intensity together with a 4-fold reduction in the emission lifetime using Bloch surface wave mediated fluorescence microscopy. The considered designs of the resonant DM, following either band structure considerations as in [25,26,30] or absorption-based optimization [31–33], are usually done to obtain a sharp resonance resulting in a large field enhancement at the free interface. However, this is not recommended in biological fluorescence microscopy where damage effects such as irreversible photobleaching of the fluorescent molecules, will be amplified proportionally to this local field enhancement. Moreover, discrepancies between theory and experiment are often observed in these large filed enhancement and are mainly explained by the illumination bandwidths [34] or the fabrication tolerances in terms of thickness or refractive index [35]. For the latter, we reported that, with the actual thin film deposition techniques, with in situ optical control, even a required thickness tolerance for such multilayer, below 1% for a structure designed to support a field enhancement of 10^4, is not a limitation [35].

However, as stated above, the intrinsic angular excitation beam divergence due to the use of high numerical aperture objective is a predominant limitation in the case of commercial TIRF-M. Furthermore, unlike in sensing application, where we search for the sharpest and strongest resonances, in fluorescence imaging, resonances with field enhancement of a few tenths but with a larger angular acceptance will be more appropriate, at least to avoid excessive photobleaching of the fluorescent particles and limit the excitation beam divergence impact. Moreover, as fluorescence is collected through the same objective than the one used for evanescent field generation, other limitation factors should be taken into account such as the optical transmission efficiency of the multilayer. These limitations were nicely discussed in [36,37].

In this paper, we first reviewed the impact of the angular divergence over the BSW resonance and we introduced a corrective term for the fluorescence collection through the stack. Still observing disagreements between the expected fluorescence efficiency and the measured one, we tackled the issue in term of resonant dielectric multilayer design. Adapting even further the absorption-based optimization, introduced in [31–33] and illustrated in Fig. 1(a-c), we investigated the impact of the imaginary part of the refractive index k of the adjacent layer to the free interface. Indeed, this k is a key parameter fixing the maximum field enhancement achievable. We introduce here our design and illustrate the use of such dedicated resonant stack in TIRF-M over model samples of tagged beads.

Optics EXPRESS

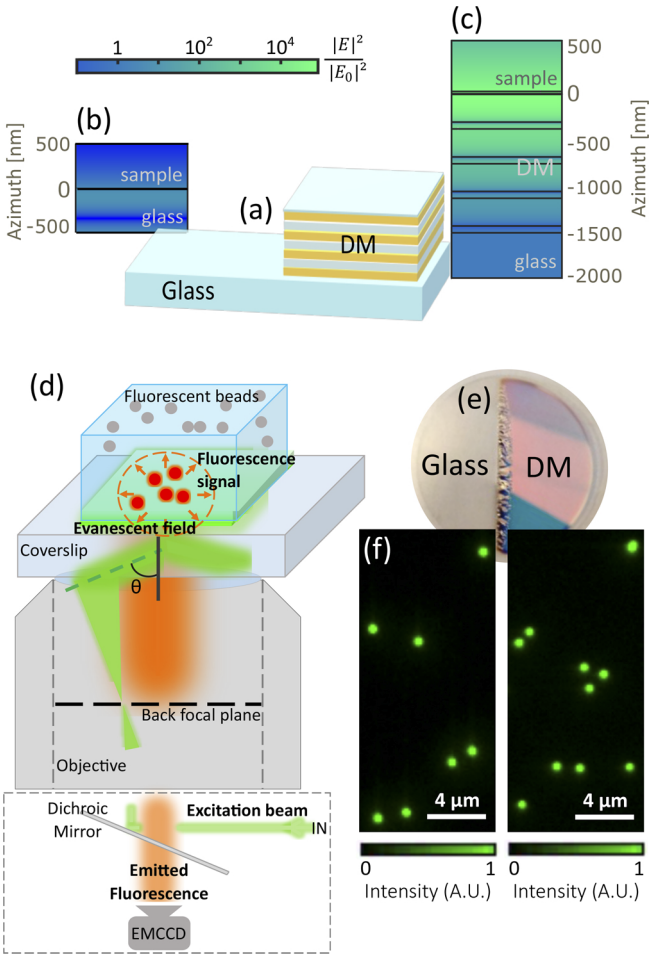

Fig. 1. (a) Scheme of a glass coverslip coated with a resonant dielectric multilayer (DM), made of a succession of two materials with low L (gray blocks) and high H (orange blocks) refractive indices. The design was done for a 561 nm laser line at an incident angle of 68° and a TE polarization for an expected resulting field enhancement of about 10^4 in the plane wave limits. (b) Calculated electromagnetic field distribution in the logarithmic scale (map) through glass material and the biological sample. (c) Same numerical study through the DM_{LH4} coating containing 4 pairs of L and H layers with a total thickness of 1542 nm. The interfaces of each materials layers are represented by black lines. (d) Experimental configuration based on an objective-based TIRF microscope: the fluorescent particles closer to the coverslip are excited by the evanescent wave (green) and the collected signal (orange) passes through the objective. (e) Example of a glass coverslip half-coated with the DM_{LH4} (f) with associated beads fluorescent maps over both regions of the coverslip.

Optics EXPRESS

2. Results and discussion

Methods and materials used to obtain the following results are detailed in Supplement 1.

2.1. Angular divergence of objective based TIRF-M strongly deteriorates performances of the resonant stack

In this study, resonant DM consists of an alternation of quarter-wave layers of SiO_2 and Nb_2O_5, which are respectively low (L) and high (H) refractive index materials, ending with an absorbing layer of SiO_x (Fig. 1(a)). In our first attempt, the DM was designed considering SiO_2 as the absorbing layer, in order to fulfill biocompatibility requirements (named hereafter DM_{LHi}, i corresponding to the number of LH pairs). Thicknesses of the different thin films were then calculated in order to generate BSW for a 561 nm excitation illumination beam with an incident angle $\theta = 68° > \theta_c$, considering that the surrounding sample material has a refractive index $n_m = 1.35$. In our numerical design, the imaginary part of the dissipating layer was fixed at $k = 10^{-5}$ to best fit the SiO_2 refractive index. In the following, we will perform a detailed numerical study of the fluorescence enhancement generated by these DM_{LHi}. We will then compare the calculated enhancement values to the one found experimentally using a commercially available TIRF-M (Nikon Ti-Eclipse), schematized in Fig. 1(d). Figure 1(b)-(c) exhibit the distribution of the excitation electric field, normalized to the initial field $|E(\theta = 68°)|^2/|E_0|^2$ under the plane wave condition, for a classical glass coverslip (Fig. 1(b)) and for a DM_{LH4} coated coverslip. The DM_{LH4}, containing four pairs of L and H refractive index layers (LH4), is supposedly the optimum structure [31]. In this configuration, we calculated a 6.10^4 fold increase of the evanescent excitation field intensity occurring at the designed coverslip/sample interface (Fig. 1(c)).

Once fabricated, as shown in Fig. 1(e), we tested the DM_{LH4} coverslip using 200 nm diameter fluorescent beads immersed in a liquid solution of a refractive index equal to 1.35. As shown in Fig. 1(d), the microscope is designed to focus a 561 nm excitation beam at the back focal plane of a 100x, 1.49 NA objective in order to obtain a parallel excitation beam on the sample. The TIR angle is reached by adjusting the radial position of the focused beam on the back focal plane. Thanks to the NA of the objective, the incident angle θ can be shifted from 0 to $\theta_{NA} = sin^{-1}(NA/n_{glass})$. Fluorescent signal emitted by beads is then collected through the objective via an Electron Multiplying CCD camera. Figure 1(f) represents fluorescence images of beads deposited on the DM_{LH4} (Fig. 1(f), right) or glass (Fig. 1(f), left) coverslip regions illuminated under the resonant conditions (i.e. $\lambda_{exc} = 561$ nm and $\theta = 68°$). We did not observe any differences in emission intensity from both sides of the coverslip despite the 6.10^4-fold numerically predicted on DM_{LH4} vs glass. This revealed us that a drastic attenuation of the BSW resonance is generated through the used commercial microscope set up design.

In a previous study, such a field enhancement ($>10^4$) was only reported with excitation spectral bandwidth lower than 1 pm and excitation angular divergence below 0.02 mrad [34]. Since in commercial microscopes, TIRF illumination is achieved by means of lasers, we discarded the effect of the spectral bandwidth as a possible explanation and we focused only on the illumination angular divergence dependency. As an indication, in the presented DM_{LH4} coverslip, the angular full width at half maximum (FWHM) of the absorption resonance peak is estimated to be 2 μrad. Unfortunately, in commercial microscope, the excitation beam is often spread angularly, as illustrated in Fig. 2(a) with a total angular divergence ($\Delta\theta$) ranging from 10 to 40 mrad (i.e., 5000 to 20000 times higher than the expected FWHM of the DM_{LH4} resonant peak).

In order to quantify the effect of such angular divergence on the evanescent excitation enhancement, we led numerical simulations by considering a gate function H (see Eq. (1) with a

Optics EXPRESS

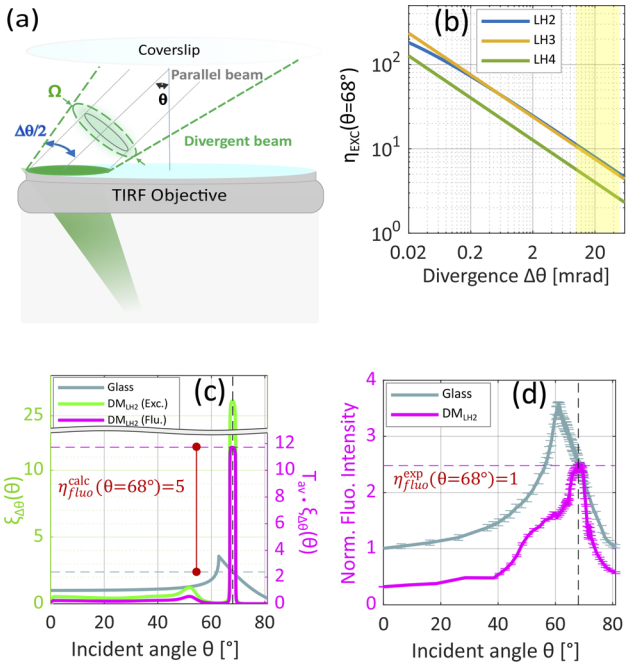

Fig. 2. (a) Schematic of an excitation laser beam presenting a divergence of $\Delta\theta$ (green dotted line) and parallel beam (gray line). (b) Numerical calculation of the local field enhancement factor versus $\Delta\theta$ in the logarithmic scale for DM_{LHi} stacks with i ranging from 2 to 4. The yellow region represents $\Delta\theta$ range on the used TIRF. (c) Numerical calculation of the incident angular dependency for the excitation $\xi_{\Delta\theta}(\theta)$ (green line) and fluorescence intensities (pink line) for DM_{LH2} coating. The blue line gives the glass response for comparison. (d) Experimental measurements of beads emitted fluorescence signal versus incident angle both on the DM_{LH2} (pink line) and glass (blue line) coverslip regions normalized to the initial intensity.

width equal to the angular divergence $\Delta\theta$ centered around the incident angle, θ.

$$H(\theta) = \begin{cases} 0 & \text{if } \theta - \frac{\Delta\theta}{2} < \theta < \theta + \frac{\Delta\theta}{2} \\ \frac{1}{\Delta\theta} & \text{if } \theta \in [\theta - \frac{\Delta\theta}{2}; \theta + \frac{\Delta\theta}{2}] \end{cases} \tag{1}$$

We defined the solid angle of the excitation beam as $\Omega = 2\pi(1 - cos\frac{\Delta\theta}{2})$.

The angular dependency of the electric field for a divergent beam is then expressed as $\xi_{\Delta\theta}(\theta)$ by the following equation :

$$\xi_{\Delta\theta}(\theta) = \frac{|E(\theta)_{\Delta\theta}|^2}{|E_0|^2} = \frac{1}{|E_0|^2} \int (|E(\theta - \Omega)|^2 . H(\Omega)) . d\Omega \tag{2}$$

In parallel, we defined a new parameter η_{exc} as the ratio of the electric field measured at the DM_{LHi}/sample interface to the one measured at the glass/sample interface.

$$\eta_{exc}(\theta) = \frac{\xi_{\Delta\theta}(\theta)_{DM}}{\xi_{\Delta\theta}(\theta)_{glass}} \tag{3}$$

In Fig. 2(b), we calculated the evolution of η_{exc} at the resonant angle ($\theta = 68°$) as a function of the beam divergence for DM_{LHi} structures exhibiting increasing number of LH layers i from 2 to

Optics EXPRESS

4. As expected, a significant decrease of the field enhancement is observed when the exciting beam divergence increases. Intriguingly, the most enhancing structures (i.e. highest LH numbers as in [31]) show the fastest decrease in η_{exc} with increasing $\Delta\theta$. Based on the measurements on the commercial TIRF microscope (see Supplement 1 for details), the laser beam divergence is evaluated to vary between 5 mrad and 30 mrad (yellow gap in the Fig. 2(b)). Interestingly, we observe that, under these conditions, the DM_{LH2} structure is expected to enhance more than the DM_{LH4}. However, η_{exc} does not exceed more than 10-fold in the considered divergence region, that is 30 times less than the estimated η_{exc} for a collimated beam.

2.2. DM transmission adds constraints on the fluorescence detection with objective based TIRF-M

As stated in the introduction, commercial TIRF microscopes are objective based, inducing excitation and emission paths to be the same but with opposite direction. The fluorescence emitted by the sample has to cross the coverslip before being collected by the objective, see Fig. 1(d), which imposes that the detected fluorescence intensity will depend on the transmission efficiency of the DM. Therefore, in a view to use such DM_{LHi} coverslips for enhanced fluorescence TIRF microscopy and to be able to directly compare experimental to theoretical enhancements, we also mapped their transmission efficiency T_{av} according to Eq. (4) as a function of the emission wavelengths λ_i and the collection angles $\theta_i \in [0, \theta_{NA}]$ fixed by the numerical aperture of the objective (i.e. $0° < \theta_{em} < 81°$).

$$T_{av} = \frac{1}{\theta_{NA}.(\lambda_2 - \lambda_1)} \int_0^{\theta_{NA}} \int_{\lambda_1}^{\lambda_2} T(\theta_{em}, \lambda_{em}) d\theta d\lambda \tag{4}$$

The numerical maps obtained for the different DM used here are represented in Fig. S1 in Supplement 1. The transmission map of the DM_{LH2} structure (Fig. S1(b) in Supplement 1) shows that, under our experimental conditions, only 45% of the total fluorescence light is transmitted through the microscope again 96% for glass coverslip (See Fig. S1(a) in Supplement 1). We performed the same calculations for increasing numbers of LH layers and we observed, as expected, that the transmission decreases with increasing LH numbers (see Fig. S2 in Supplement 1), confirming the DM_{LH2} to be more suitable for the TIRF-M configuration. Based on this observation, we introduced a fluorescence enhancement factor defined as:

$$\eta_{fluo}(\theta_{exc}) = \eta_{exc}(\theta_{exc}).T_{av} \tag{5}$$

We calculated the excitation enhancement (η_{exc}) and the fluorescence enhancement (η_{fluo}) at different excitation angles (θ_{exc}) using the angular divergence ($\Delta\theta = 10.0 \pm 0.9$ mrad) determined experimentally. Figure 2(c) predicted, for the DM_{LH2}, enhancement factors at resonance of respectively $\eta_{exc}(\theta = 68°) = 11 \pm 1$ and $\eta_{fluo}(\theta = 68°) = 5.0 \pm 0.4$.

In regard to these results, we fabricated a DM_{LH2} and conducted experimental measurements of fluorescence intensity changes as a function of excitation angle, using 200 nm fluorescently labelled latex beads. Figure 2(d) shows the changes in the beads fluorescence intensity using DM_{LH2} versus glass coverslip (see also Visualization 1). Using the DM_{LH2} coverslip, a fluorescence signal enhancement is occurring at the expected resonance angle $\theta = 68°$. However, with respect to the glass coverslip, we observed an experimental enhancement $\eta_{fluo}^{exp} = 1.0 \pm 0.1$, at the resonance angle, that is again far from the calculated one $\eta_{fluo}^{calc} = 5.0 \pm 0.4$. This suggests that, besides the instrumental constraints, there is a particular parameter which influences the sensitivity of the resonant structure.

Optics EXPRESS

2.3. *Fluorescence enhancement can be predicted by controlling the absorption in the top layer*

All numerical calculations that have been carried out up to now relied on an approximated values of the extinction coefficient of the SiO_2 thin layers equal to k=10^{-5}. Influence of this parameter on η_{fluo} was studied (Fig. 3). Figures 3(a,b) depict the variations of calculated η_{fluo} as a function of k for the DM_{LH2} case. It can be immediately seen that small changes in k induced drastic decreases in the fluorescence enhancement. Indeed, a deviation of $3.5.10^{-5}$ from the reference k induces a loss of about 80% in η_{fluo}^{calc} value (see Fig. 3(b)). This points out the absolute necessity to experimentally determine and control the k value of the top layer in order to correctly predict the enhancement. With actual spectral techniques, k values can be measured with a precision up to 10^{-4}. Furthermore, knowing that by increasing the k of the top layer, we will decrease the enhancement but expand the angular acceptance of the DM resonance [38], we therefore totally re-thought the DM coverslip design and optimization (See Supplement 1).

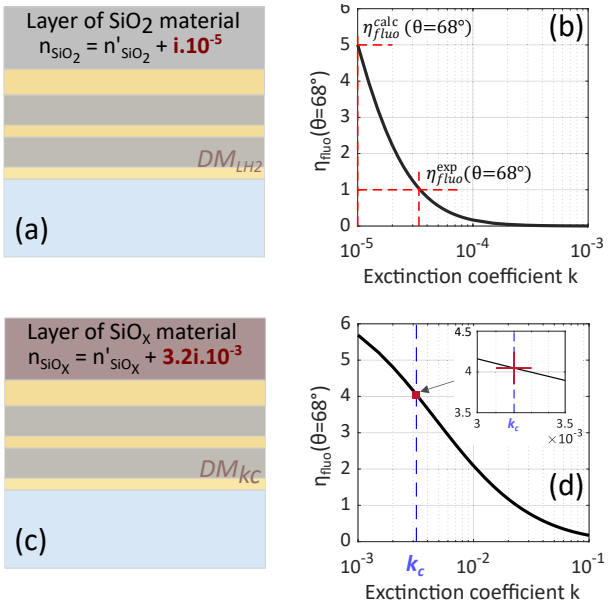

Fig. 3. (a) The studied DM_{LH2} stack includes an absorbing SiO_2 layer of extinction coefficient k = 10^{-5}. (b) Variation of the calculated fluorescence enhancement factor with k values ranging from 10^{-5} to 10^{-3}. (c) & (d) Same numerical study for the proposed DM_{kc} stack with k-controlled absorbing SiO_x layer of $k_c = (3.2 \pm 0.1).10^{-3}$ over k values ranging from 10^{-3} to 10^{-1}.

First, in order to obtain a measurable k values of the top layer, we controlled the oxidization level of the last layer, moving from SiO_2 used in the DM_{LHi} coverslips (Fig. 3(a)) to SiO_x (Fig. 3(c)). Optimization of the deposition parameters was carried out by monitoring *in situ* the transmission a single layer during deposition and adjusting the plasma assistance parameters until reaching the desired k value (See Supplement 1). The resulting complex refractive index of this single layer was then accurately extracted by spectrophotometry and estimated to be $n = 1.602 + i.(3.2 \pm 0.1).10^{-3}$ at 561 nm. This controlled SiO_x layer was then deposited as the last layer of the microscopy-dedicated DM_{k_c} coverslip.

Secondly, in order to limit the impact of the incident angular divergence and improve the fluorescence collection efficiency, we also modified the quarter wave multilayer part below the last layer as presented in Fig. 1(a). Such a DM resonance consists of both field enhancement

Optics EXPRESS

and a localized absorption at the operating conditions, the new design of the stack consisted therefore of entering several weighted targets to reach the dedicated experimental conditions, i.e. a relatively large absorption; a spectral model for resonances; a broader angular model to numerically force the convergence on structures with good angular tolerance and finally a field maximization at the free interface of the structure in contact with the biological environment. We thus obtained sets of solutions that met the optical specifications. In a last step, we sorted the solutions by taking into account the thin film fabrication strains.

We thus obtained a DM_{k_c} coverslip with a controlled k together with an angular tolerance improved by a factor of 10 (Fig. S3 in Supplement 1) and an improved transmission efficiency (Fig. S2 in Supplement 1). We estimated an average transmission of 58% for the presented DM_{k_c} coverslip against 45% for the best DM_{LHi} coverslip (Fig. S1(e) and Fig. S2 in Supplement 1). Based on this new structure, we calculated the changes in η_{fluo} as a function of the extinction coefficient for DM_{k_c} coverslips (Fig. 3(d) and Fig. S4(b) in Supplement 1). We clearly evidenced

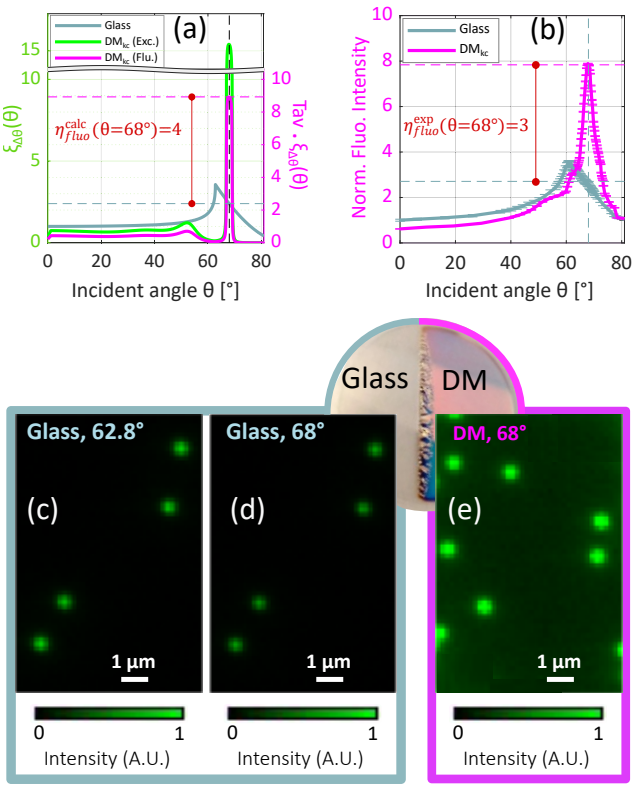

Fig. 4. (a) Numerical calculation of the incident beam angular dependency of the excitation $\xi_{\Delta\theta}(\theta)$ (green line) and fluorescence signal intensity (pink line) for DM_{k_c} coating compared to the glass material (blue line). A fluorescent enhancement factor of 4 is predicted at 68°. (b) Experimental measurement of the fluorescence intensity emitted by beads on the surface of DM_{k_c} (pink line) and glass coverslip (blue line) normalized to the initial intensity versus incident angle shows a fluorescence enhancement factor of 3. (c) Images of fluorescent beads recorded on the surface of glass coverslip at the critical beam angle θ_c of 62.8° where the excitation reaches its maximum intensity (d) same beads exited at 68°. (e) Images of beads on the surface of DM_{k_c} exited at 68°. See also Visualization 1 and Visualization 2 showing the fluorescence intensity as a function of the incident angle for both glass and DM_{k_c} substrates.

Optics EXPRESS

that, unlike DM_{LHi} coverslips, the signal enhancement factor is now not severely impacted by a slight deviation in k and stays close to 4 within the experimental tolerance over k (inset of Fig. 3(d)).

We then performed numerical calculations of the enhancements (η_{exc} and η_{fluo}) and estimated their changes with the excitation angle (Fig. 4(a)), taking into account experimental excitation divergence and calculated DM_{k_c} transmission (58%). Calculations predicted an η_{fluo}=4.0±0.2, that we quantified experimentally, using the same approach than previously with DM_{LH2}. From Fig. 4(b), an experimental η_{fluo}=3.0±0.1 is observed at $\theta = 68°$, which is in line with the predicted value.

Interestingly, not only we observed an $\eta_{fluo} = 3$ at 68°, but also a $\simeq 2$ times enhancement with respect to the maximal enhancement on glass surface at the total reflection angle ($\theta_c = 62.8°$), confirming the advantage of using our DM coverslips for objective based TIRF microscopy, as illustrated in Figs. 4(c)-e (see also Visualization 1 & Visualization 2).

3. Conclusion

In our work, a biocompatible coverslip based on dedicated resonant dielectric multilayers (DM) for TIRF microscopy was designed to locally enhance the excitation evanescent field. In order to be able to predict experimental enhancements, we performed numerical simulations taking into account the different obstacles due to the experimental commercial set-up and DM_{LH_i} coverslips, namely, beam divergence and transmission efficiency. However, we observed huge discrepancies between prediction and experimentation over the fluorescence enhancement in the case of the DM_{LH_i}, that we identified to be due to the steep variation of the η_{fluo} with the k. This steep variation makes this approach almost impossible to have quantitatively predictable η_{fluo} while designing the DM_{LH_i} coverslips. To overcome this issue, we designed a dielectric multilayer resulting in broad angular resonance peak with a 10 times larger FWHM and with a controlled extinction coefficient using an absorbing top layer of SiO_x ($k_c = (3.2 \pm 0.1).10^{-3}$). With the proposed solution, we experimentally observed a 3-fold increase of the fluorescence signal enhancement factor which is close to the predicted enhancement factor equal to 4. Therefore, with the dedicated dielectric multilayer, we expect to achieve a fluorescent enhancement factor of 10 in TIRF-M systems with controlled divergences of about 0.1°. This new design opens large perspectives in the field of evanescent waves enhancement for objective based commercial TIRF microscopes and associated super-resolution techniques such as PALM, STORM and structured illumination TIRF.

Funding. Centre National de la Recherche Scientifique.

Acknowledgments. This work was sponsored by the CNRS - Centre National de la Recherche Scientifique, through the MITI- Mission for Transversal and Interdisciplinary Initiatives 2017 and the AAP 80|PRIME 2019. Anita Mouttou's Ph.D is granted by CNRS. The authors acknowledge Dr D. Muriaux for fruitful discussions and the Centre d'Etudes des Maladies Infectieuses et Pharmacologie Anti-Infectieuse (CEMIPAI) and Montpellier Ressources Imagerie (MRI) facilities for access to the commercial TIRF-M. The authors thank Olivier Hector for his help during deposition of the dielectric structures. C. Favard is a member of the CNRS consortium GDR Imabio.

Disclosures. The authors declare no conflicts of interest.

Data availability. The data that support the findings of this study are available from the corresponding authors upon reasonable request.

Supplemental document. See Supplement 1 for supporting content.

References

1. D. Axelrod, N. L. Thompson, and T. P. Burghardt, "Total internal inflection fluorescent microscopy," J. Microsc. **129**(1), 19–28 (1983).
2. E. Betzig, G. H. Patterson, R. Sougrat, O. W. Lindwasser, S. Olenych, J. S. Bonifacino, M. W. Davidson, J. Lippincott-Schwartz, and H. F. Hess, "Imaging intracellular fluorescent proteins at nanometer resolution," Science **313**(5793), 1642–1645 (2006).

Optics EXPRESS

3. M. J. Rust, M. Bates, and X. Zhuang, "Sub-diffraction-limit imaging by stochastic optical reconstruction microscopy (storm)," Nat. Methods **3**(10), 793–796 (2006).
4. K. Inamdar, C. Floderer, C. Favard, and D. Muriaux, "Monitoring hiv-1 assembly in living cells: Insights from dynamic and single molecule microscopy," Viruses **11**(1), 72 (2019).
5. K. Inamdar, F.-C. Tsai, R. Dibsy, A. de Poret, J. Manzi, P. Merida, R. Muller, P. Lappalainen, P. Roingeard, J. Mak, P. Bassereau, C. Favard, and D. Muriaux, "Full assembly of hiv-1 particles requires assistance of the membrane curvature factor irsp53," eLife **10**, e67321 (2021).
6. C. Floderer, J.-B. Masson, E. Boilley, S. Georgeault, P. Merida, M. El Beheiry, M. Dahan, P. Roingeard, J.-B. Sibarita, C. Favard, and D. Muriaux, "Single molecule localisation microscopy reveals how hiv-1 gag proteins sense membrane virus assembly sites in living host cd4 t cells," Sci. Rep. **8**(1), 16283 (2018).
7. G. W. Ashdown, G. L. Burn, D. J. Williamson, E. Pandžic, R. Peters, M. Holden, H. Ewers, L. Shao, P. W. Wiseman, and D. M. Owen, "Live-cell super-resolution reveals f-actin and plasma membrane dynamics at the t cell synapse," Biophys. J. **112**(8), 1703–1713 (2017).
8. C. V. Carman, "Overview: imaging in the study of integrins," Methods Mol. Biol. **757**, 159–189 (2012).
9. N. Bourg, C. Mayet, G. Dupuis, T. Barroca, P. Bon, S. Lécart, E. Fort, and S. Lévêque-Fort, "Direct optical nanoscopy with axially localized detection," Nat. Photonics **9**(9), 587–593 (2015).
10. M. Brunstein, M. Teremetz, K. Hérault, C. Tourain, and M. Oheim, "Eliminating unwanted far-field excitation in objective-type tirf. part i. identifying sources of nonevanescent excitation light," Biophys. J. **106**(5), 1020–1032 (2014).
11. M. Oheim, "Imaging transmitter release. ii. a practical guide to evanescent-wave imaging," Lasers Med. Sci. **16**(3), 159–170 (2001).
12. J. Homola, S. S. Yee, and G. Gauglitz, "Surface plasmon resonance sensors: review," Sens. Actuators, B **54**(1-2), 3–15 (1999).
13. J. R. Lakowicz, "Radiative decay engineering 3. surface plasmon-coupled directional emission," Anal. Biochem. **324**(2), 153–169 (2004).
14. I. Gryczynski, J. Malicka, Z. Gryczynski, and J. R. Lakowicz, "Surface plasmon-coupled emission with gold films," J. Phys. Chem. B **108**(33), 12568–12574 (2004).
15. D. G. Zhang, X. Yuan, and A. Bouhelier, "Direct image of surface-plasmon-coupled emission by leakage radiation microscopy," Appl. Opt. **49**(5), 875 (2010).
16. K. Balaa, V. Devauges, Y. Goulam, V. Studer, S. Lévêque-Fort, and E. Fort, "Live cell imaging with surface plasmon-mediated fluorescence microscopy," Proc. SPIE **7367**, 736710 (2009).
17. E. L. Moal, E. Fort, S. Lévêque-Fort, F. P. Cordelières, M.-P. Fontaine-Aupart, and C. Ricolleau, "Enhanced fluorescence cell imaging with metal-coated slides," Biophys. J. **92**(6), 2150–2161 (2007).
18. J. Y. Ye and M. Ishikawa, "Enhancing fluorescence detection with a photonic crystal structure in a total-internal-reflection configuration," Opt. Lett. **33**(15), 1729 (2008).
19. M. Ballarini, F. Frascella, F. Michelotti, G. Digregorio, P. Rivolo, V. Paeder, V. Musi, F. Giorgis, and E. Descrovi, "Bloch surface waves-controlled emission of organic dyes grafted on a one-dimensional photonic crystal," Appl. Phys. Lett. **99**(4), 043302 (2011).
20. R. Badugu, K. Nowaczyk, E. Descrovi, and J. R. Lakowicz, "Radiative decay engineering 6: Fluorescence on one-dimensional photonic crystals," Anal. Biochem. **442**(1), 83–96 (2013).
21. A. Angelini, E. Enrico, N. D. Leo, P. Munzert, L. Boarino, F. Michelotti, F. Giorgis, and E. Descrovi, "Fluorescence diffraction assisted by bloch surface waves on a one-dimensional photonic crystal," New J. Phys. **15**(7), 073002 (2013).
22. K. Toma, E. Descrovi, M. Toma, M. Ballarini, P. Mandracci, F. Giorgis, A. Mateescu, U. Jonas, W. Knoll, and J. Dostálek, "Bloch surface wave-enhanced fluorescence biosensor," Biosens. Bioelectron. **43**, 108–114 (2013).
23. E. Descrovi, D. Morrone, A. Angelini, F. Frascella, S. Ricciardi, P. Rivolo, N. D. Leo, L. Boarino, P. Munzert, F. Michelotti, and F. Giorgis, "Fluorescence imaging assisted by surface modes on dielectric multilayers," Eur. Phys. J. D **68**(3), 53 (2014).
24. M. C. D. Santos, R. Déturche, C. Vézy, and R. Jaffiol, "Axial nanoscale localization by normalized total internal reflection fluorescence microscopy," Opt. Lett. **39**(4), 869 (2014).
25. K. Ray, R. Badugu, and J. R. Lakowicz, "Bloch surface wave-coupled emission from quantum dots by ensemble and single molecule spectroscopy," RSC Adv. **5**(67), 54403–54411 (2015).
26. A. Sinibaldi, N. Danz, E. Descrovi, P. Munzert, U. Schulz, F. Sonntag, L. Dominici, and F. Michelotti, "Direct comparison of the performance of bloch surface wave and surface plasmon polariton sensors," Sens. Actuators, B **174**, 292–298 (2012).
27. S. D. Choudhury, R. Badugu, and J. R. Lakowicz, "Directing fluorescence with plasmonic and photonic structures," Acc. Chem. Res. **48**(8), 2171–2180 (2015).
28. A. L. Lereu, M. Zerrad, A. Passian, and C. Amra, "Surface plasmons and bloch surface waves: Towards optimized ultra-sensitive optical sensors," Appl. Phys. Lett. **111**(1), 011107 (2017).
29. T. G. Mayerhöfer, S. Pahlow, and J. Popp, "Structures for surface-enhanced nonplasmonic or hybrid spectroscopy," Nanophotonics **9**(4), 741–760 (2020).
30. F. Michelotti, R. Rizzo, A. Sinibaldi, P. Munzert, C. Wächter, and N. Danz, "Design rules for combined label-free and fluorescence bloch surface wave biosensors," Opt. Lett. **42**(14), 2798 (2017).

Optics EXPRESS

31. C. Ndiaye, F. Lemarchand, M. Zerrad, D. Ausserré, and C. Amra, "Optimal design for 100% absorption and maximum field enhancement in thin-film multilayers at resonances under total reflection," Appl. Opt. **50**(9), C382 (2011).
32. A. L. Lereu, M. Zerrad, M. Petit, F. De Fornel, and C. Amra, "Multi-dielectric stacks as a platform for giant optical field," Proc. SPIE **9162**, 916219 (2014).
33. A. L. Lereu, M. Zerrad, C. Ndiaye, F. Lemarchand, and C. Amra, "Scattering losses in multidielectric structures designed for giant optical field enhancement," Appl. Opt. **53**(4), A412 (2014).
34. M. Zerrad, A. L. Lereu, C. N'diaye, F. Lemarchand, and C. Amra, "Bandwidths limitations of giant optical field enhancements in dielectric multi-layers," Opt. Express **25**(13), 14883 (2017).
35. A. L. Lereu, F. Lemarchand, M. Zerrad, D. Niu, V. Aubry, A. Passian, and C. Amra, "Sensitivity of resonance properties of all-dielectric multilayers driven by statistical fluctuations," Opt. Express **27**(21), 30654 (2019).
36. F. Michelotti and E. Sepe, "Anisotropic fluorescence emission and photobleaching at the surface of one-dimensional photonic crystals sustaining bloch surface waves. i. theory," J. Phys. Chem. C **123**(34), 21167–21175 (2019).
37. E. Sepe, A. Sinibaldi, N. Danz, P. Munzert, and F. Michelotti, "Anisotropic fluorescence emission and photobleaching at the surface of one-dimensional photonic crystals sustaining bloch surface waves. ii. experiments," J. Phys. Chem. C **123**(34), 21176–21184 (2019).
38. C. Amra, M. Zerrad, F. Lemarchand, A. Lereu, A. Passian, J. A. Zapien, and M. Lequime, "Energy density engineering via zero-admittance domains in all-dielectric stratified materials," Phys. Rev. A **97**(2), 023819 (2018).